6.15 CHARACTERIZING ATMOSPHERIC TURBULENCE WITH GPS

Frank Kleijer (1) *, Pedro Elósegui (1, 2), James L. Davis (1)
(1) Harvard-Smithsonian Center for Astrophysics, Cambridge, MA, USA
(2) Institut d'Estudis Espacials de Catalunya/CSIC, Barcelona, Spain

1. INTRODUCTION

The Global Positioning System (GPS), originally designed for navigation purposes, has shown its capabilities for use in atmospheric studies for over a decade now (e.g., Bevis et al. 1992). Atmospheric delays of the GPS signals, caused by the atmospheric refractivity along the ray path to a ground-based receiver, are used as tracers of atmospheric densities. The delay caused by the electrically neutral atmosphere consist of a wet and hydrostatic component and is often referred to as tropospheric delay, because the troposphere is responsible for most of this delay. Usually, Zenith Tropospheric Delays (ZTDs), are estimated by mapping slant delays (i.e., delays along the ray paths) to zenith-equivalent values by a zenith-angle-dependent mapping function. Mapping functions depend on (mean) atmospheric conditions and usually assume a horizontally layered (homogeneous) atmosphere. This way a single parameter, the ZTD, describes the mean atmospheric state. If we subtract the hydrostatic zenith delay, which is well predictable when accurate pressure values are known, the remaining part of the ZTD can be attributed to water vapor and is often used as observation for atmospheric studies. This single parameter does however not reflect any heterogeneous fluctuations in the atmosphere caused by turbulence.

Although parameterization of all fluctuations is impossible since, even in a network of receivers, this would lead to an underdetermined set of equations, we can derive a stochastic model for the fluctuations if we assume Kolmogorov turbulence. In fact, we could estimate the fluctuations if we added extra zero-mean pseudo-observations (soft constraints) for these fluctuations with their corresponding covariance matrix (Kleijer 2004). If we knew the scaling of the covariance matrix, these soft constraints could improve the positioning precision for static applications, since atmospheric turbulence is believed to be a dominating error source. This scaling would represent the degree of heterogeneity, or turbulence, present in the atmosphere.

This paper describes a method for estimating this turbulence variance scale factor with a single GPS receiver. The application we have in mind is that of an accurate, independent, continuous, all-weather, inexpensive, near-real-time, passive remote-sensing technique for measuring atmospheric turbulence strength.

Instantaneous measurements of refractive-index fluctuation variations are important for a variety of atmosphere problems, and could potentially improve weather forecasts. Numerical weather prediction models, used for either short or long-term predictions, can treat the meteorology on scales down to a few kilometers with reasonable accuracy, but have neither the temporal nor spatial resolution required to describe the turbulent interaction that occurs in the boundary layer (Wyngaard 1992). The current inability to couple small-scale atmospheric processes in the boundary layer to large-scale numerical weather prediction models can significantly degrade performance of the latter (Beljaars 1995). This inability stems, from lack of reliable measurements of instantaneous refractive-index fields in the boundary layer (Wyngaard et al. 2001). With its low-cost user systems, sensing the atmosphere with GPS, using its carrier-beat phase observables, would seem to offer possibilities for near-real-time monitoring of atmospheric turbulence over dense spatial fields.

In the section that follows we introduce the GPS observation equations. In Sect. 3, we develop three stochastic turbulence models. Section 4 deals with the technique of Variance Component Estimation (VCE) and describes the VCE observation model that we used, based on the observation equations of Sect. 2 and the stochastic models of Sect. 3. In Sect. 5, we present preliminary results of applying this method to a GPS data set from a station near Mt. Washington, New Hampshire. We discuss the results of this study in Sect. 6.

2. GPS OBSERVATION EQUATIONS

The GPS observes at two frequencies: $f_1 = 154 \cdot 10.23$ MHz ≈ 1.57 GHz and $f_2 = 120 \cdot 10.23$ MHz ≈ 1.23 GHz. The observation equation for the GPS carrier-beat phase observable $\phi_{s,f}(k)$ for epoch $k = 1, ..., b$, satellite $s = 1, ..., m_k$, and frequency $f = 1, 2$ is:

$$\begin{aligned} \phi_{s,f}(k) \;=\; & a_{s,f} \;+\; \rho_s(k) \;-\; \delta s_s(k) \;+\; \tau_s(k) \\ & +\, \delta r_{,f}(k) \;+\; \mu_f \imath_s(k) \;+\; \epsilon_{s,f}(k). \end{aligned} \tag{1}$$

(See, e.g.: Hofmann-Wellenhof et al. 1992; Teunissen and Kleusberg 1998.) In Eq. (1), $a_{s,f}$ is the non-integer phase ambiguity, an integer ambiguity lumped with initial phase offsets at receiver and satellite; $\rho_s(k)$ is the range between receiver and satellite; $\delta s_s(k)$ is the satellite clock error lumped with assumed equal satellite hardware delays for both frequencies; $\tau_s(k)$ is the tropospheric delay; $\delta r_{,f}(k)$ is the receiver clock error lumped with a frequency-dependent hardware-delay term; $\mu_f \imath_s(k)$ is the ionospheric delay; and $\epsilon_{s,f}(k)$ is a zero-mean random observation error term. All terms are in metric units.

* *Corresponding author address:* Frank Kleijer, Harvard-Smithsonian Center for Astrophysics, 60 Garden Street, Cambridge, MA 02138, USA; e-mail: fkleijer@cfa.harvard.edu.

The observations are corrected for a-priori values of known or modeled errors such as phase-center variations, solid earth tides, phase wind-up, and a-priori tropospheric delays. The latter at least include the hydrostatic delays, but often also wet delays, leaving only residual wet delays as troposphere parameters. We can also correct the observations for known ranges and satellite clock errors. Equation (1) then still holds, but instead of ranges and satellite clock errors, it contains range errors and differential satellite clock errors as parameters. The ranges can be computed from known receiver and satellite coordinates, for example, from Precise Orbit Determination (POD) from global solutions of GPS data, such as those produced by the International GPS Service (IGS) (Beutler et al. 1999). Satellite clock errors can, analogously, be obtained from IGS solutions. Since these two parameters cannot be separated in a single-receiver set-up, they will be lumped into a parameter

$$\varrho_s(k) \doteq \rho_s(k) - \delta s_s(k), \tag{2}$$

where $\doteq$ denotes 'by definition.' The corrected phase observations are also referred to as prefit residuals.

The dispersiveness of the ionosphere is expressed in the scale factor μ_f. We may assign $\mu_1 = f_2/f_1$ and $\mu_2 = f_1/f_2$, or any multiple of these two values. A linear combination of the observables at both frequencies can be formed as:

$$\begin{aligned} \phi_{s,\ell}(k) &\doteq \mu_1\phi_{s,2}(k) - \mu_2\phi_{s,1}(k) \\ &= a_{s,\ell} + \gamma_\ell\varrho_s(k) + \gamma_\ell\tau_s(k) \\ &\quad + \delta r_{,\ell}(k) + \epsilon_{s,\ell}(k), \end{aligned} \tag{3}$$

giving an ionosphere-free observable. The index ℓ indicates a linear combination, and $\gamma_\ell \doteq \mu_1 - \mu_2$. We will assume μ_1 and μ_2 are chosen such that $\gamma_\ell = 1$. An example of ionosphere-free prefit residuals is shown in Fig. 1.

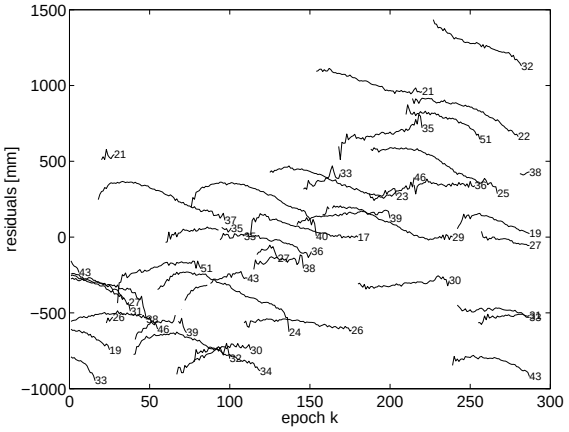

FIG. 1: Ionosphere-free prefit residuals of a 24-hour GPS data set sampled at 300-s intervals (see below). The residuals have been corrected for receiver clock errors for clarity. GPS satellites are identified by their Pseudo Random Noise (PRN) code number (shown to the right of each line).

If we have m_k satellites at epoch k, $m_k - 1$ single-differenced observables can be formed:

$$\Delta\phi_{s,\ell}(k) = \Delta a_{s,\ell} + \Delta\varrho_s(k) + \Delta\tau_s(k) + \Delta\epsilon_{s,\ell}(k). \tag{4}$$

These single differences are formed between satellites; usually, when processing baselines, the term 'single difference' refers to differences between receivers. In Eq. (4) there are no receiver-clock errors since they are common to all ionosphere-free observables at epoch k. These equations are underdetermined. If we have b epochs of data and if $m = m_1 = \cdots = m_b$, there are $b(m-1)$ observations, $m-1$ ambiguities, $b(m-1)$ lumped range and satellite clock parameters, and $b(m-1)$ troposphere parameters. To create redundancy we have to make some assumptions. One possibility is to assume that the parameters $\Delta\varrho_s(k)$ are constant in time. In fact this is a reasonable assumption if the a-priori corrections to the ranges and satellite clock errors are unbiased. In this case we have to lump them with the ambiguities to generally constant parameters, reducing the total number of parameters by $b(m-1)$. An alternative is to assume them linearly changing in time, reducing the number of parameters by only $(b-1)(m-1)$ instead. The usual method of reducing the number of troposphere parameters is assuming that the tropospheric delays for a certain epoch are products of a single zenith delay and a mapping function. The number of troposphere parameters is then reduced to one ZTD per epoch. For sufficiently short periods the number of parameters could even further be reduced to one ZTD per batch. Sophisticated mapping functions exist for large zenith angles (e.g., Niell 1996), but below 75° a simple secant function probably suffices for our application.

A least-squares estimation of parameters is now possible if we have a covariance matrix of the observables. The noise of the observables consists of random noise $\Delta\epsilon_{s,\ell}(k)$, errors in the a-priori corrections of the ranges and satellite clock errors, and atmospheric turbulence. It is in the last type of noise we are interested in this study.

3. TURBULENCE NOISE

We consider the tropospheric delay caused by turbulence to be the zero-mean difference between the actual slant delay τ and a mapped zenith delay τ^z:

$$\delta\tau(\alpha_s, z_s) \doteq \tau(\alpha_s, z_s) - M(z_s)\tau^z, \tag{5}$$

where α_s is the azimuth of satellite s, and $M(z_s)$ is the mapping function for satellite s as function of zenith angle z_s. In short-hand notation we write: $\delta\tau_s \equiv \delta\tau(\alpha_s, z_s)$, $\tau_s \equiv \tau(\alpha_s, z_s)$, and $M_s \equiv M(z_s)$, where $\equiv$ is the notation for 'is equivalent with.' If we use a zenith-delay mapping as parameterization of the slant tropospheric delay, the term $\delta\tau_s$ remains as an error term to be modeled stochastically. A zenith-equivalent delay can be defined as:

$$\tau_s^z \doteq M_s^{-1}\tau_s = 10^{-6}\int_0^\infty N(\mathbf{r}_s(h))\,dh, \tag{6}$$

where $N(\mathbf{r}_s(h))$ is the refractivity along the ray path, $\mathbf{r}_s(h)$ is the position vector for a point along the ray path, and h is the height above the receiver in meters. Using a mapping function assumes a horizontally layered atmosphere where the refractivity is a function of height alone. The zenith-equivalent delay in the zenith direction itself will be written as τ_0^z, and the corresponding direction vector by $\mathbf{r}_0$.

With the equation

$$(a-b)(c-d) = \frac{1}{2}[(a-d)^2+(b-c)^2-(a-c)^2-(b-d)^2], \quad (7)$$

the turbulence covariance between any two directions i and j can now be found (Emardson and Jarlemark 1999; Kleijer 2004):

$$\begin{aligned}
&\mathbf{E}\{\delta\tau_i\ \delta\tau_j\} = \\
&\mathbf{E}\{[\tau_i - M_i\tau^z][\tau_j - M_j\tau^z]\} = \\
&M_iM_j\ \mathbf{E}\{[M_i^{-1}\tau_i - \tau^z][M_j^{-1}\tau_j - \tau^z]\} = \\
&M_iM_j\ \mathbf{E}\{[\tau_i^z - \tau_0^z][\tau_i^z - \tau_0^z]\} = \\
&M_iM_j\ 10^{-12}\ \mathbf{E}\{\int_0^\infty\int_0^\infty [N(\mathbf{r}_i(h_1)) - N(\mathbf{r}_0(h_1))] \\
&\qquad \times[N(\mathbf{r}_j(h_2)) - N(\mathbf{r}_0(h_2))]\ dh_1dh_2\} = \\
&\frac{1}{2}M_iM_j\ 10^{-12}\int_0^\infty\int_0^\infty [D_N^{i0} + D_N^{0j} \\
&\qquad -D_N^{ij} - D_N^{00}]\ dh_1dh_2,
\end{aligned} \quad (8)$$

where $\mathbf{E}\{.\}$ denotes the mathematical expectation, and

$$\begin{aligned}
D_N^{ij} &\equiv D_N(\mathbf{r}_i(h_1), \mathbf{r}_j(h_2)) \\
&\doteq <[\ N(\mathbf{r}_i(h_1)) - N(\mathbf{r}_j(h_2))\ ]^2> \\
&= \mathbf{E}\{[\ N(\mathbf{r}_i(h_1)) - N(\mathbf{r}_j(h_2))\ ]^2\}
\end{aligned} \quad (9)$$

is a short-hand notation for the refractivity structure function. We assumed the property of ergodicity, that is, time averages $< . >$ equal statistical means.

Kolmogorov turbulence predicts the structure function to be a power-law function (Tatarski 1961):

$$D_N^{ij} = C_N^2\ |\mathbf{r}_i - \mathbf{r}_j|^p, \quad (10)$$

with $p = 2/3$, and C_N^2 [m^{-p}] a refractivity constant. This power-law function was however derived for horizontal refractivity differences. There may be a very different height dependency. Therefore we investigate the performance of three different models that take into account a different height dependency: The uniform weighting-model (u), the exponential-weighting model (e), and the layer model (l); see appendix.

Each of the models ($* = u, e, l$) can be written as

$$\mathbf{E}\{\delta\tau_i\ \delta\tau_j\} = \sigma_{2,*}^2 Q_{2,*}^u\{i,j\}, \quad (11)$$

where $Q_{2,*}^u\{i,j\}$ is the $\{i,j\}$th element of the cofactor matrix $Q_{2,*}^u$. (The upper-index u indicates 'undifferenced.') The cofactor matrix depends on geometry only. The turbulence variance factor $\sigma_{2,*}^2$ is considered a turbulence strength parameter, which we intend to estimate.

Values for the elements of the cofactor matrix for the exponential-weighting model are shown in Fig. 2 for a certain geometry. (This geometry is unusual, but instructive.)

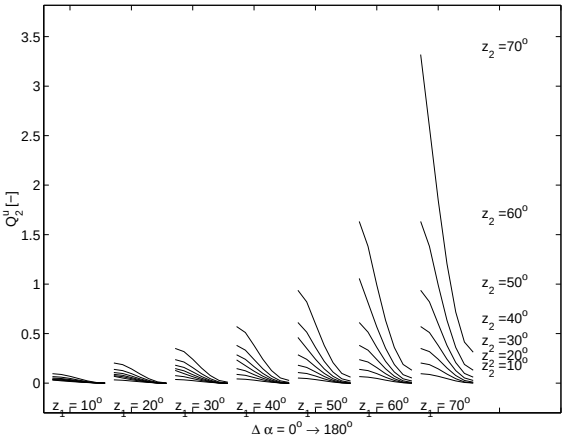

FIG. 2: Values of the undifferenced turbulence cofactor matrix for the exponential-weighting model. A geometry is assumed with zenith angles z_1 and z_2 of 10° to 70° in steps of 10° and azimuth differences $\Delta\alpha$ of 0° to 180° in steps of 30° for each zenith-angle combination; lines between points are shown for clarity.

This figure shows that for larger zenith angles the turbulence (co-)variance increases rapidly. For increasing azimuth differences the covariance, and therefore the correlation, decreases. These characteristics hold for all three models.

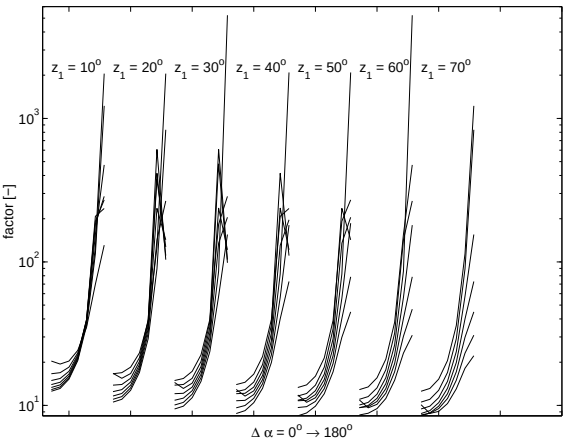

FIG. 3: Values of turbulence cofactor matrix ratios of the layer model and the exponential-weighting model: $Q_{2,l}^u\{i,j\}/Q_{2,e}^u\{i,j\}$. Same geometry as in Fig. 2.

Figure 3 shows ratios of the elements of the cofactor matrix in the layer model and the exponential-weighting model. The values are on average about a factor 15 smaller for the exponential-weighting model for actual satellite geometries at Mt. Washington (see below), but for azimuths of 180° this factor can increase up to a few thousand. The uniform-weighting model is closer to the exponential-weighting model. It has on average values of about one-fifth of the layer-model values.

4. VARIANCE COMPONENT ESTIMATION

Although turbulence noise is expected to be the dominant error source, there may be other error sources. Often the (ionosphere-free) phase observables are assumed uncorrelated for channel-related observation noise. (GPS receivers usually measure on 12 channels to a maximum of 12 satellites.) If the observation noise is equal for all channels, the covariance matrix for epoch k reads:

$$\mathbf{D}\{\epsilon_{,\ell}(k)\} = \sigma_1^2 I_{m_k}, \tag{12}$$

where $\epsilon_{,\ell}(k) \doteq [\epsilon_{1,\ell}(k), ..., \epsilon_{m_k,\ell}(k)]'$, $\mathbf{D}\{.\} \doteq \mathbf{E}\{(. - \mathbf{E}\{.\})(. - \mathbf{E}\{.\})'\}$ denotes the mathematical dispersion, σ_1^2 is the variance of the observation noise, and I_{m_k} is an m_k-by-m_k identity matrix. (We use $'$ for the transpose of a vector or matrix.) We assume that errors in the satellite clocks and orbits can be subsumed here as well.

If the total noise for the undifferenced observations $\phi_{,\ell}(k) \doteq [\phi_{1,\ell}(k), ..., \phi_{m_k,\ell}(k)]'$ at epoch k consists of observation noise $\epsilon_{,\ell}(k)$ and turbulence noise $\delta\tau(k) \doteq [\delta\tau_1(k), ..., \delta\tau_{m_k}(k)]'$, our total stochastic model reads:

$$\mathbf{D}\{\phi_{,\ell}(k)\} = \sigma_1^2 I_{m_k} \; + \; \sigma_2^2 Q_2^u(k), \tag{13}$$

where $Q_2^u(k) = \mathbf{E}\{\delta\tau(k)\,\delta\tau(k)'\}$ follows from the geometry at epoch k as in Eq. (28): The matrix $Q_2^u(k)$ is epoch dependent because of the changing satellite configurations; in each of the three models it depends only on the receiver-satellite directions. In Eq. (13), we dropped the model indicator $* = u, e, l$ for readability.

Equation (13) describes the assumed covariance matrix of the undifferenced observables. The GPS observation equations of Eq. (4) are however single-differenced. The single-difference transformation for all observations of epoch k reads: $\Delta\phi_{,\ell}(k) = S(k)'\phi_{,\ell}(k)$, with single-difference transformation matrix

$$S(k)' \doteq \begin{bmatrix} 1 & & & -1 & & & \\ & \ddots & & \vdots & & & \\ & & 1 & -1 & & & \\ & & & -1 & 1 & & \\ & & & \vdots & & \ddots & \\ & & & -1 & & & 1 \end{bmatrix}, \tag{14}$$

which has the -1s at any of the columns. But this column, which refers the the pivot satellite, is part of the definition of $S(k)$; it is associated with epoch k. If we observe to m_k satellites in epoch k, $S(k)'$ has size $(m_k - 1)$-by-m_k.

The stochastic model for the single-differenced observables follows from the propagation law of (co)variances:

$$\mathbf{D}\{y(k)\} \doteq Q_y(k) = \sigma_1^2 Q_1(k) \; + \; \sigma_2^2 Q_2(k), \tag{15}$$

where $y(k) \equiv \Delta\phi_{,\ell}(k)$ is used as a shorter notation for the single-differenced observables, and $Q_1(k) \doteq S(k)'S(k)$ and $Q_2(k) \doteq S(k)'Q_2^u(k)S(k)$ are transformed cofactor matrices. The corresponding functional model reads:

$$\mathbf{E}\{y(k)\} = A(k)\, x, \tag{16}$$

with $A(k)$ the (partial) design matrix for epoch k, and x the vector with parameters, containing lumped ambiguities, ZTDs, and, if so desired, linearly changing (range/satellite clock) parameters. If we stack the observations of all epochs in one vector, $y = [y(1)', ..., y(b)']'$, use the notation $A = [A(1)', ..., A(b)']'$, and assume the observables to be uncorrelated in time, $Q_i = \text{diag}[Q_i(1), ..., Q_i(b)]$, the observation model for estimating parameters reads:

$$\mathbf{E}\{y\} = A\, x \quad ; \quad \mathbf{D}\{y\} = Q_y. \tag{17}$$

The least-squares corrections to the observations are: $\hat{\varepsilon} = [\hat{\varepsilon}(1)', ..., \hat{\varepsilon}(b)']' = P_A^{\perp} y$, with $P_A^{\perp} = I - A(A'Q_y^{-1}A)^{-1}A'Q_y^{-1}$ a projector that projects on the orthogonal subspace of A. Least-squares estimates of the variance factors σ_1^2 and σ_2^2 can be found by Variance Component Estimation (VCE) (e.g.: Kenselaar 1993; Koch 1999). The variance estimates follow from solving a set of normal equations $N\hat{\sigma} = \beta$, where $\hat{\sigma} = [\hat{\sigma}_1^2, \hat{\sigma}_2^2]'$, and

$$\begin{aligned} N_{ij} &= \frac{1}{2}\text{tr}(Q_y^{-1}P_A^{\perp}Q_iQ_y^{-1}P_A^{\perp}Q_j); \\ \beta_i &= \frac{1}{2}y'Q_y^{-1}P_A^{\perp}Q_iQ_y^{-1}P_A^{\perp}y, \end{aligned} \tag{18}$$

with, in this case, $i, j = 1, 2$. We used the notation $\text{tr}(.)$ for the trace of a matrix. Solving the normal equations involves iterations because they are in terms of Q_y, for which a priori values of the variance factors are required. The covariance matrix of the variance factor estimates is the inverse of the normal matrix: $Q_{\hat{\sigma}} = N^{-1}$. The covariance matrix of the estimated variance factors depends on the estimated variance factors themselves, since the normal matrix also depends on them. The VCE formulas take more computation time than simple least-squares estimation of parameters would because of the iterations and since a set of normal equations is to be solved involving cofactor matrix products for each element of the normal matrix. Especially for large numbers of observations the inversion of the covariance matrix takes a lot of computation time, even if we do not actually compute the inverse but use Cholesky decompositions and substitutions instead. The block-diagonal structure of the cofactor matrices, and therefore also of the total covariance matrix, saves however considerate computation time since smaller partial covariance matrices are inverted.

In the special case of just one variance factor, the amount of computations is reduced further. If the observation noise can be neglected, so that all noise is attributed to turbulence noise, the computation of the turbulence variance factor reduces to: $\hat{\sigma}_2^2 = \beta/N$, with

$$\begin{aligned} N &= \frac{1}{2}\sigma_2^{-4}\, r; \\ \beta &= \frac{1}{2}\sigma_2^{-4} \sum_{k=1}^{b} \hat{\varepsilon}(k)'Q_2(k)^{-1}\hat{\varepsilon}(k), \end{aligned} \tag{19}$$

and $r = \sum(m_k - 1) - n$ the redundancy if n is the number

of parameters. Or simply:

$$\begin{aligned} \hat{\sigma}_2^2 &= \sum_{k=1}^{b} \hat{\varepsilon}(k)' Q_2(k)^{-1} \hat{\varepsilon}(k)/r; \\ \hat{\sigma}^2_{\hat{\sigma}_2^2} &= 2\,\hat{\sigma}_2^4/r. \end{aligned} \tag{20}$$

5. PRELIMINARY RESULTS

In this section, we present results using data from a site in a regional GPS network that we established near Mt. Washington, New Hampshire, at 19–26 October 2000, for atmospheric studies (Elósegui and Davis 2001). We used the GIPSY-OASIS software package (Webb and Zumberge 1993), GPS satellite PODs and clocks from the IGS/Jet Propulsion Laboratory (JPL) global solutions, and site position from our processing, to compute ionosphere-free prefit residuals once every five minutes (see Fig. 1; clear outliers were removed). This low sampling rate was dictated by the sampling interval of JPL's most precise PODs. The preliminary experimental results of this section concern the GPS data collected on October 21, 2000.

The observation model included one ZTD per epoch and constant parameters in which ambiguities, ranges, and satellite clocks are lumped. The turbulence variance factors were estimated with a moving window technique to obtain estimates for each batch of $b = 12$ epochs, which corresponds to one hour of data. With this technique in each new batch the data of the next epoch is added and the data of the first epoch is removed. The estimates are therefore correlated.

First, with the general VCE formulas, both σ_1^2 and σ_2^2 were estimated. The estimates of σ_1^2 showed very low precision. From simulations it could be seen that this is only the case for small values of σ_1^2. Therefore, in new computations only the turbulence variance factors were estimated with Eq. (20). These estimates showed very little difference with the previously acquired ones.

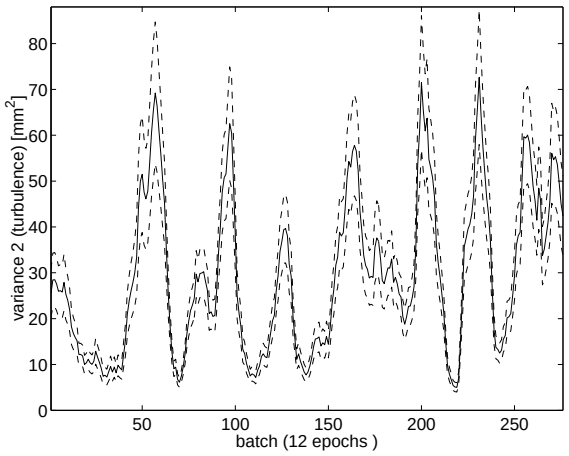

FIG. 4: Estimated turbulence variance factor for the Mt. Washington data set. Layer model. Batch size: 12 epochs. Dashed: 1-σ error lines.

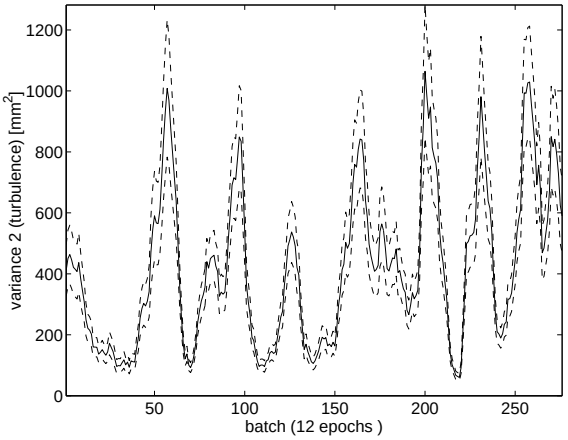

FIG. 5: Estimated turbulence variance factor for the Mt. Washington data set. Exponential-weighting model. Batch size: 12 epochs. Dashed: 1-σ error lines.

Figures 4 and 5 show the turbulence variance-factor estimates for each batch, using the layer model and the exponential-weighting model respectively. The difference in scaling is clear, and can directly be attributed to the different scaling in the cofactor matrices. Apart from that, both models result in a similar behavior of the estimates, despite the theoretically large differences.

The precision of the variance-factor estimates depends on the stochastic model, the satellite geometry, the batch size, parameterization, and zenith cut-off angle. Hardly any difference was however found between the stochastic models, and the precision showed only little variation for the satellite geometry at Mt. Washington. For a zenith cut-off angle of 80° and a batch size of 12 epochs, the standard deviation of the estimated turbulence variance factor is about 19% of the estimated variance factor itself. Decreasing the zenith cut-off angle to 70° gives a percentage of about 24. In other words, the precision decreases because the number of observations decreases, but low-elevation satellites are not vital. In fact, it is better not to use them, because GPS potential error sources, such as multipath and phase-center variations, are sensitive to observations at large zenith angles; also the zenith-delay mapping requires a good mapping function. Increasing the batch size to 24 epochs gives a percentage of 13. Larger batches are therefore preferred, but only if the turbulence variance factor does not vary much within the batch. Figure 6 shows the estimates when a batch size of 24 is used. The larger batch size has a smoothing effect, but also results in larger variance-factor estimates, probably because of an insufficient functional model. Therefore, a higher sampling is required, not longer duration of the batches.

6. DISCUSSION

The stochastic models as described in this paper have properties we would expect them to have. The decreasing correlation between increasing azimuths seems

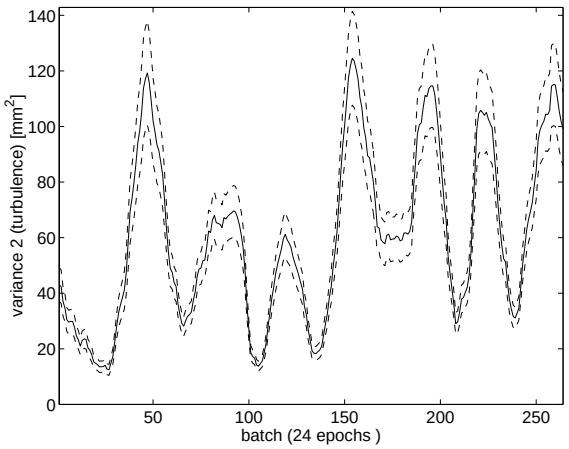

FIG. 6: Estimated turbulence variance factor for the Mt. Washington data set. Layer model. Batch size: 24 epochs. Dashed: 1-σ error lines.

intuitively correct and the decrease in variance toward larger zenith angles is known in the GPS community (e.g.: Rothacher et al. 1997).

Estimation of the turbulence variance factor seems to be possible with high precision. The preliminary computations of the Mt. Washington data set show temporal variations larger than the formal precision. These variations are therefore likely to be real variations.

Except for a scaling constant $C^2_{N,*}$, the estimated variance factors showed to be relatively insensitive to the chosen stochastic model. This scaling constant is yet to be interpreted. Note that the variance factors also depend on the scaling by the GPS data processing software when forming ionosphere-free observations.

An internal quality indicator is to be found that shows which model performs best. Although observations to low-elevation satellites are not strictly needed for precise estimation of the turbulence variance, they may play a role in the distinction of the performance of the three models. Also the power p, as used in each of the models, should be considered a parameter for fine-tuning. Hypothesis testing and VCE are the mathematical tools we have at hand for internal validation.

We intend to process data of more stations at different types of locations and under different atmospheric conditions. We also intend to use higher sampling rates by interpolating or estimating satellite clock errors (using a network of receivers). We are currently considering experimental validation of our method using independent observational techniques and numerical methods such as Large-Eddy Simulations (LES).

APPENDIX

In this appendix we show the three turbulence models: The uniform-weighting model, the exponential-weighting model, and the layer model.

The first model assumes C^2_N to be equal to a constant $C^2_{N,u}$ for h_1 and h_2 smaller than some height H, say the scale height of water vapor ($\sim$ 2 km), and zero elsewhere (Emardson and Jarlemark 1999; Kleijer 2004). We refer to this model as the uniform-weighting model. The double integral over the structure function yields:

$$\begin{aligned}&\int_0^\infty\int_0^\infty D_N^{ij}\,dh_1dh_2 = \\ &C^2_{N,u}\int_0^H\int_0^H |\mathbf{r}_i(h_1)-\mathbf{r}_j(h_2)|^p\,dh_1dh_2 = \\ &C^2_{N,u}\,H^{p+2}F_u(i,j;p),\end{aligned} \tag{21}$$

with

$$\begin{aligned}F_u(i,j;p) \doteq \int_0^1\int_0^1 &|x_1^2\sec^2(z_i)+x_2^2\sec^2(z_j) \\ &-2x_1x_2\sec(z_i)\sec(z_j)\cos(\theta_{ij})|^{\frac{p}{2}}\,dx_1dx_2\end{aligned} \tag{22}$$

a dimensionless function, and θ_{ij} the angle between directions i and j. We used the change of variables $x_1 \doteq h_1/H$ and $x_2 \doteq h_2/H$. Note that $F_u(i,i;p) = \sec^p(z_i)\cdot F_u(0,0;p)$ and $F_u(0,0;p) = 2(p+1)^{-1}(p+2)^{-1}$. Because this function cannot be computed analytically for $i \neq j$, we have to rely on numerical integration or, to save computation time, approximating summations.

The second model assumes a (probably more realistic) exponentially decaying function for the refractivity structure function resulting from an exponentially decaying C^2_N (Gradinarsky 2002; Stoew 2004). This exponential-weighting model yields:

$$\begin{aligned}&\int_0^\infty\int_0^\infty D_N^{ij}\,dh_1dh_2 = \\ &C^2_{N,e}\int_0^\infty\int_0^\infty |\mathbf{r}_i(h_1)-\mathbf{r}_j(h_2)|^p \\ &\qquad\cdot\exp(-(h_1+h_2)/H)\,dh_1dh_2 = \\ &C^2_{N,e}\,H^{p+2}F_e(i,j;p),\end{aligned} \tag{23}$$

with

$$\begin{aligned}F_e(i,j;p) \doteq \int_0^\infty\int_0^\infty &|x_1^2\sec^2(z_i)+x_2^2\sec^2(z_j)- \\ &2x_1x_2\sec(z_i)\sec(z_j)\cos(\theta_{ij})|^{\frac{p}{2}}\cdot\exp(-x_1-x_2)\,dx_1dx_2.\end{aligned} \tag{24}$$

This function has properties: $F_u(i,i;p) = \sec^p(z_i)\cdot F_u(0,0;p)$ and $F_u(0,0;p) = \int_0^\infty x^p\exp(-x)dx \doteq \Gamma(p+1)$, where $\Gamma(.)$ is the gamma function. For $i \neq j$, the function $F_e(i,j;p)$ has to be computed numerically also.

The third model assumes there is correlation between refractivity values within limited height differences, but not beyond. We refer to this model as the layer model because the atmosphere is assumed to be layered and turbulence between layers is assumed to be negligible. This model yields (Davis and Elósegui 2001):

$$\begin{aligned}&\int_0^\infty\int_0^\infty D_N^{ij}\,dh_1dh_2 = \\ &\int_0^\infty C^2_{N,l}(h)\cdot\Delta H\cdot|\mathbf{x}_i(h_1)-\mathbf{x}_j(h_2)|^p\,dh = \\ &\Delta H\int_0^\infty C^2_{N,l}(h)\,h^p\,dh\cdot F_l(i,j;p),\end{aligned} \tag{25}$$

with $\mathbf{x}_i$ the horizontal component of $\mathbf{r}_i$, and

$$\begin{aligned}F_l(i,j;p) \doteq |\tan^2(z_i)+\tan^2(z_j) \\ -2\tan(z_i)\tan(z_j)\cos(\alpha_{ij})|^{\frac{p}{2}},\end{aligned} \tag{26}$$

where $\alpha_{ij} \doteq \alpha_j - \alpha_i$ is the azimuth difference ($\Delta\alpha$) of directions i and j, and ΔH is the layer thickness. Contrary to the previous models no (numerical) integration is needed. Special cases are: $F_l(i,0;p) = \tan^p(z_i)$ and $F_l(i,i;p) = 0$.

Each of the models ($* = u, e, l$) can be written as

$$\mathbf{E}\{\delta\tau_i \; \delta\tau_j\} = \sigma^2_{2,*} Q^u_{2,*}\{i,j\}, \tag{27}$$

if we define the $\{i,j\}$th element of the cofactor matrix $Q^u_{2,*}$ as

$$\begin{aligned} Q^u_{2,*}\{i,j\} \doteq M_i M_j \; [&F_*(i,0;p) + F_*(0,j;p) \\ &-F_*(i,j;p) - F_*(0,0;p)] \,, \end{aligned} \tag{28}$$

and assign:

$$\begin{aligned} \sigma^2_{2,u} &= \frac{1}{2} 10^{-12} \; C^2_{N,u} \; H^{p+2}; \\ \sigma^2_{2,e} &= \frac{1}{2} 10^{-12} \; C^2_{N,e} \; H^{p+2}; \\ \sigma^2_{2,l} &= \frac{1}{2} 10^{-12} \; \Delta H \int_0^\infty C^2_{N,l}(h) \; h^p \; dh. \end{aligned} \tag{29}$$

Acknowledgments

This research was supported by grant ATM-0222531 of the National Science Foundation (NSF).

REFERENCES

Beljaars, A.C.M., 1995: The parameterization of surface fluxes in large-scale models under free convection. *Quart. J. Roy. Meteor. Soc.*, **121**, 255–270.

Beutler, G., M. Rothacher, S. Schaer, T.A. Springer, J. Kouba, and R.E. Neilan, 1999: The International GPS Service (IGS): An interdisciplinary service in support of earth sciences. *Sat. Dynam., Orbit Analy. Comb. Space Tech. Adv. Space Research*, **23 (4)**, 631–653.

Bevis, M., S. Businger, T.A. Herring, C. Rocken, R.A. Anthes, and R. Ware, 1992: GPS meteorology: Remote sensing of atmospheric water vapor using the Global Positioning System. *Journal of Geophysical Research (D)*, **97**, 15787–15801.

Davis, J.L., and P. Elósegui, 2001: *A new method for measuring turbulence in a local airspace using a ground-based Global Positioning System receiver*. Space Geodesy Group Internal Report, Smithsonian Astrophysical Observatory, Harvard-Smithsonian Center for Astrophysics, Cambridge.

Elósegui, P., and J.L. Davis, 2001: *Sensing atmospheric structure: GPS water-vapor tomography to improve severe weather forecasts*. Smithsonian Astrophysical Observatory IR&D Project Report (available at URL: cfa-www.harvard.edu/space_geodesy).

Emardson, T.R., and P.O.J. Jarlemark, 1999: Atmospheric modelling in GPS analysis and its effect on the estimated geodetic parameters. *Journal of Geodesy*, **73**, 322–331.

Gradinarsky, L.P., 2002: *Sensing atmospheric water vapor using radio waves*. PhD dissertation, Chalmers University of Technology, Göteborg.

Hofmann-Wellenhof, B., H. Lichtenegger, and J. Collins, 1992: *GPS: Theory and practice*. 3rd ed., Springer-Verlag, Wien.

Kenselaar, F., 1993: *Variance component estimation: A review*. Internal report, Mathematical Geodesy and Positioning, Delft University of Technology, Delft.

Kleijer, F., 2004: *Troposphere modeling and filtering for precise GPS leveling*. PhD dissertation, Delft University of Technology, Delft.

Koch, K.-R., 1999: *Parameter estimation and hypothesis testing in linear models*. 2nd ed., Springer-Verlag, Berlin.

Niell, A.E., 1996: Global mapping functions for the atmosphere delay at radio wavelengths. *Journal of Geophysical Research (B)*, **101**, 3227–3246.

Rothacher, M., T.A. Springer, S. Schaer, and G. Beutler, 1997: Processing strategies for regional GPS networks. Presented at *IAG General Assembly 1997, Rio, Brazil, September 3–9, 1997*.

Stoew, B., 2004: *Description and analysis of data and errors in GPS meteorology*. PhD dissertation, Chalmers University of Technology, Göteborg.

Tartarski, V.I., 1961: *Wave propagation in a turbulent medium*. Translated from Russian by R.A. Silverman. McGraw-Hill, New York.

Teunissen, P.J.G., and A. Kleusberg, 1998: GPS observation equations and positioning concepts. In: *GPS for geodesy*. 2nd ed., Springer-Verlag, Berlin.

Webb, F.H., and J.F. Zumberge, 1993: *An introduction to the GIPSY/OASIS-II*. JPL Publ. D-11088.

Wyngaard, J.C., 1992: Atmospheric turbulence. *Annu. Rev. Fluid Mech.*, **24**, 205–233.

Wyngaard, J.C., N. Seaman, S.J. Kimmel, M. Otte, X. Di, and K.E. Gilbert, 2001: Concepts, observations, and simulation of refractive index turbulence in the lower atmosphere. *Radio Science*, **36**, 643–669.